UW Biostatistics Working Paper Series

1-19-2011

A Flexible Spatio-Temporal Model for Air Pollution: Allowing for Spatio-Temporal Covariates

Johan Lindstrom
Lund University, johanl@math.lth.se

Adam A. Szpiro
University of Washington, aszpiro@u.washington.edu

Paul D. Sampson
University of Washington - Seattle Campus, pds@stat.washington.edu

Lianne Sheppard
University of Washington, sheppard@u.washington.edu

Assaf Oron
University of Washington, assaf@uw.edu

See next page for additional authors

Authors
Johan Lindstrom, Adam A. Szpiro, Paul D. Sampson, Lianne Sheppard, Assaf Oron, Mark Richards, and Tim Larson

A FLEXIBLE SPATIO-TEMPORAL MODEL FOR AIR POLLUTION: ALLOWING FOR SPATIO-TEMPORAL COVARIATES

By Johan Lindström*,†, Adam A Szpiro*, Paul D Sampson*, Lianne Sheppard*, Assaf Oron*, Mark Richards*, and Tim Larson*

*University of Washington** *and Lund University*†

Abstract Given the increasing interest in the association between exposure to air pollution and adverse health outcomes, the development of models that provide accurate spatio-temporal predictions of air pollution concentrations at small spatial scales is of great importance when assessing potential health effects of air pollution. The methodology presented here has been developed as part of the Multi-Ethnic Study of Atherosclerosis and Air Pollution (MESA Air), a prospective cohort study funded by the US EPA to investigate the relationship between chronic exposure to air pollution and cardiovascular disease. We present a spatio-temporal framework that models and predicts ambient air pollution by combining data from several different monitoring networks with the output from deterministic air pollution model(s). The model can accommodate arbitrarily missing observations and allows for a complex spatio-temporal correlation structure.

We apply the model to predict long-term average concentrations of gaseous oxides of nitrogen (NO_x) — one of the primary pollutants of interest in the MESA Air study — during a ten year period in the Los Angeles area, based on measurements from the EPA Air Quality System and MESA Air monitoring. The measurements are augmented by a spatio-temporal covariate based on the output from a source dispersion model for traffic related air pollution (Caline3QHC) and the model is evaluated using cross-validation. The predictive ability of the model is good with cross-validated R^2 of approximately 0.7 at subject sites.

The incorporation of a dispersion model output into the overall prediction model was feasible, but the particular implementation of Caline3QHC used here did not improve predictions in a model that also includes road information. However, excluding the road information the inclusion of model output improves predictions and we find some evidence that the source dispersion model can replace road covariates.

The model presented in this paper has been implemented in an R package, `SpatioTemporal`, which will be available on CRAN shortly.

1. Introduction. There is growing epidemiological evidence of an association between exposure to air pollution and adverse health outcomes. The seminal cohort studies were based on assigning exposures using area-wide monitored concentrations in different geographic regions (Dockery et al., 1993; Pope et al., 2002). While straightforward to implement based on regulatory monitoring data, this approach fails to take advantage of variation between individuals living in the same geographic region and may be subject to unmeasured confounding by region.

More recent cohort studies have assigned individual concentrations based on estimates of intra-urban variations in ambient concentrations using nearest-monitor interpolation (Miller et al., 2007; Basu et al., 2000; Ritz et al., 2006; Goss et al., 2004), "land use" regression estimates based on Geographic Information System (GIS) covariates (Hoek et al., 2008; Brauer et al., 2003; Jerrett et al., 2005a), geostatistical methods such as kriging (Jerrett et al., 2005b; Kunzli et al., 2005), and semi-parametric smoothing in space and/or time (Kunzli et al., 2005; Puett et al., 2009).

The primary objective of the work described in this paper is develop methods that can be used to produce accurate spatio-temporal predictions of ambient air pollution concentrations for subjects in the Multi-Ethnic Study of Atherosclerosis and Air Pollution (MESA Air). The primary pollutants of interest for MESA Air are particulate matter with aerodynamic diameter less than 2.5 μm ($PM_{2.5}$) and gaseous oxides of nitrogen (NO_x).

MESA Air is a cohort study funded by the Environmental Protection Agency (EPA) with the aim of assessing the relationship between chronic exposure to air pollution and the progression of sub-clinical cardiovascular disease. The MESA Air cohort is comprised of more than 6000 male and female subjects, from six major US metropolitan areas (Los Angeles, CA; New York, NY; Chicago, IL; Minneapolis-St. Paul, MN; Winston-Salem, NC; and Baltimore, MD). The subjects cover four racial/ethnic groups (White, African-American, Hispanic, and Asian, predominantly of Chinese descent) and were aged 45-84 years and free of cardiovascular disease at baseline (see Bild et al., 2002, for details).

A primary focus of the MESA Air study is the development of accurate predictions of ambient air pollution at the home locations of study participants. Combining these predictions with subject-level data — e.g. building infiltration factors, time-activity patterns, and address history — will allow for subject-specific estimates of chronic ambient source exposure. Using subject-specific exposures, instead of simpler exposure estimates such as the regional average or nearest monitor, provides greater heterogeneity in the exposure estimates. The greater heterogeneity will improve health effect

studies by 1) allowing us to control for confounding between region where appropriate; 2) reducing measurement error from using predicted exposures (Szpiro et al., 2010b; Gryparis et al., 2009; Carroll et al., 2006); and 3) increasing study power.

The primary interest for MESA Air is predicting the chronic exposure of our subjects, but due to several considerations our statistical model needs to account for complex spatio-temporal variability in the data (see Section 3 for details). Overviews of statistical modeling approaches for spatially and spatio-temporally correlated data can be found in Cressie (1993) and Banerjee et al. (2004). For modeling of spatio-temporally correlated air pollution data, Fanshawe et al. (2008) used carefully selected covariates to eliminate the need for correlated residuals. Several different techniques that allow for complex spatio-temporal dependence structures have been proposed. Two examples are Sahu et al. (2006) and Paciorek et al. (2009), both modeling PM; however these approaches require relatively complete observation matrices. Their methods are also developed for much larger geographic regions than those of interest for MESA Air. Smith et al. (2003) handles arbitrary missing observations through an expectation-maximization (EM) algorithm, but their model does not allow for complex spatio-temporal dependencies.

An alternative to statistical modeling is to use numerical models to provide deterministic spatio-temporal predictions of air pollution (Irwin, 2002; Appel et al., 2008). However, when compared to measurements, air quality model output often shows varied prediction performance (Lindström et al., 2010; Appel et al., 2008; Hogrefe et al., 2006; Mathur et al., 2008). Integrating model output with observations in an attempt to obtain better predictions is an active field of research. Most existing studies use output from grid-based models over large geographic areas (e.g., Fuentes and Raftery, 2005; Berrocal et al., 2010; McMillan et al., 2010). Since the MESA Air modeling domains are geographically compact we have opted here to combine our observations with the output from a point prediction model (Caline3QHC, described in EPA, 1992b).

Our goal is to construct a general statistical framework that allows us to combine the EPA regulatory and MESA Air supplemental monitoring data (Cohen et al., 2009) with the output of deterministic air pollution models (EPA, 1992b). A spatio-temporal modeling framework for MESA Air has been introduced previously in Sampson et al. (2009) and Szpiro et al. (2010a). Sampson et al. (2009) predicts $PM_{2.5}$ at subject homes, using a pragmatic approach that estimates different components of the model separately and then combines these components to produce predictions. Szpiro et al. (2010a) presents a unified maximum-likelihood estimation method and

studies the statistical properties of the model as well as the added value of MESA Air supplemental monitoring using a simulation study based on a limited set of NO_x observations in Los Angeles.

This paper expands on the work of Szpiro et al. (2010a) by: 1) extending the model to include spatio-temporal covariates in order to incorporate output from the Caline3QHC deterministic prediction model; 2) applying the model to the full MESA Air NO_x dataset to generate predictions in Los Angeles; 3) reducing the computational burden by implementing profile likelihood (and restricted maximum likelihood) in order to decrease the dimension of the optimization problem and by introducing a simplification of the profile likelihood function that decreases the time required for each iteration; and 4) implementing a novel cross-validation strategy for long-term average predictions that accounts for the complex MESA Air monitoring design. The model presented in this paper has been implemented in an R package, `SpatioTemporal`, which will be available on the CRAN website shortly.

The available data are described in Section 2. These include observations from both the EPA Air Quality System (AQS) regulatory network and the MESA Air supplemental monitoring, as well as geographic covariates and output from our deterministic air pollution model. Section 3 describes the spatio-temporal model, discusses techniques for efficient parameter estimation, and describes our cross-validation approach. Different options for incorporating the output from our deterministic air pollution model are described in Section 4. In Section 5 we apply the model to NO_x data from Los Angeles and use cross-validation to assess the model's predictive ability. Section 6 discusses these results.

2. Description of Data.

2.1. *Air Quality System (AQS).* The national AQS network of regulatory monitors consists of a modest number of fixed sites that measure ambient concentrations of several different air pollutants including NO_x and $PM_{2.5}$. Many AQS sites provide hourly averages for NO_x, while monitoring of $PM_{2.5}$ is less frequent. For this study we include NO_x data from 20 AQS sites in and around Los Angeles.

Since the supplementary MESA Air monitoring is done at the 2-week timescale, we aggregate the AQS data to 2-week averages. The distribution of the resulting 2-week average NO_x concentrations is skewed, so we log-transform the 2-week averages. Examples of time series from three AQS sites are shown in Figure 1; the three sites are located in Glendora, Lynwood, and

Costa Mesa, as indicated on the map in Figure 2. Note the different seasonal patterns and mean levels in the three time series.

Due to maintenance and equipment failures there is some missing data in the AQS monitoring, resulting in a small amount of variability in the number of AQS measurements that contribute to each 2-week average. Periods with less than nine valid measurements have been excluded. This variability can result in different amounts of measurement error. For simplicity we assume a common variance for the measurement error of all AQS and MESA Air 2-week average concentrations (as in Szpiro et al., 2010a).

2.2. *MESA Air.* The AQS monitors provide data with excellent temporal resolution, but only at relatively few locations in each of the six cities in the MESA Air study. As pointed out in Szpiro et al. (2010a), potential problems with basing exposure estimates entirely on data from the AQS network are: 1) the number of locations sampled is limited; 2) the AQS network is designed for regulatory rather than epidemiology purposes and does not resolve small scale spatial variability; and 3) the network has siting restrictions that limit its ability to resolve near-road effects. To address these restrictions the MESA Air supplementary monitoring campaign was designed to provide increased diversity in geographic monitoring locations, with specific importance placed on proximity to traffic. The sampling strategy and measurement methodology is described in Cohen et al. (2009). We present a brief overview.

The MESA Air supplementary monitoring of ambient outdoor concentrations consists of three sub-campaigns: "fixed sites", "home outdoor", and "community snapshot". The campaigns collect 2-week average concentrations in each of the six study areas. The fixed and home outdoor campaigns measure $PM_{2.5}$ and gaseous co-pollutants including NO_x, while the snapshot campaign only measures NO_x and other gaseous co-pollutants. Details for the three MESA Air sub-campaigns follow.

1) The MESA Air fixed sites consist of a few monitors that provided 2-week averages during the entire MESA Air monitoring period. To allow for comparison of different monitoring protocols, at least one MESA fixed site per metropolitan area was colocated with an existing AQS monitor. 2) The home outdoor campaign was designed to obtain information about the concentration of pollution at participant homes, and consisted of a rotating set of four monitors that were placed at a subset (roughly 10%) of the participants home locations, collecting at least two 2-week averages at each site. 3) The goal of the community snapshot campaign was to collect a spatially rich dataset that could be used to model small scale spatial variability and road-

way effects; and to provide a convenient dataset to guide spatial covariate selection (Mercer et al., 2010). The community snapshot campaign provides three sets of simultaneous measurements of 2-week average concentrations at many locations, including roadway gradients, during three different seasons. The roadway gradients consisted of six monitors placed perpendicular to a major roadway (three on either side), at approximately 50, 100, and 150 meters (see Cohen et al., 2009, for details).

For this paper we restrict attention to sampling in central and costal portion of the Los Angeles basin. A summary of available data, detailing the number of monitor sites, total number of observations, the time periods of the monitoring, and some summary statistics for the observations can be found in Tables 1–2 and Figure 3. Note that one of the MESA fixed sites in the area studied in this paper is colocated with an AQS monitor.

2.3. *Geographic Information System (GIS).* To predict ambient air pollution at times and locations where we have no measurements we use a complex spatio-temporal model that includes regression with geographic covariates. Since some of the geographical variables relate to local land utilization this approach is often termed "land use" regression (LUR) (Jerrett et al., 2005b). The MESA Air study has created a comprehensive geographic database, and after a preliminary study of the data based on the snapshot campaigns, a subset of the available covariates was selected for use in the present analysis (The selection was based on a preliminary version of the results in Mercer et al., 2010). The covariates used in this paper are: 1) distance to a major road, i.e., census feature class code A1–A3 (distances truncated to be ≥ 10m and log-transformed), 2) distance to a A1 road (≥ 10m, log-transformed), 3) total length of A1 and A2 roads in a circular buffer with 300 meter radius, 4) total length of A3 roads in a 50 meter buffer, 5) distance to coast (truncated to be ≤ 15km), and 6) average population density in a 2 km buffer. These are all derived using the ArcGIS (ESRI, Redlands, CA) software package. The distance to coast and roadway variables were obtained from Tele Atlas Dynamap 2000 (Lebanon, NH), and the population density was calculated from publicly available Census Bureau data.

2.4. *Caline Dispersion Model for Air Pollution.* The geographic covariates described above are fixed in time and provide only spatial information. To aid in the spatio-temporal modeling, covariates that vary in both space and time would be valuable. One option is to integrate output from deterministic air pollution models into our spatio-temporal model. Several different air pollution models exist, and in this paper we use a slightly modified version of Caline3QHC (EPA, 1992b; Wilton et al., 2010; MESA Air Data

Team, 2010).

Caline is a line dispersion model for air pollution. Given locations of major sources and local meteorology Caline uses Gaussian dispersion model to predict how nonreactive pollutants travel with the wind away from sources. In contrast to grid-based air pollution models, Caline provides hourly estimates of air pollution at distinct points, called receptors, avoiding the change of support problem inherent in the use of grid based models (e.g. Gotway and Young, 2002; Fuentes and Raftery, 2005).

The Caline predictions we use are based on estimates of traffic density on major roads (A1, A2, and large A3) in the Los Angeles area, obtained from the Southern California Association of Governments. To account for diurnal and weekly variations in traffic patterns, a one week pattern of hourly variations was computed from data provided by the California Department of Transportation. The weekly pattern was repeated for the entire ten-year period and used to modulate the traffic density. The dispersion in Caline is driven by meteorology obtained from the LAX airport meteorology station, and complemented by upper air data from the Radiosonde Database, Earth System Research laboratory, NOAA. We used a unit emissions factor in our Caline implementation.

A final consideration for the Caline computations is the area, or buffer, around each receptor from which pollution is allowed to affect predictions at that receptor. A simplistic interpretation is that the size of the buffer determines how far we believe traffic pollution diffuses during one hour. In preliminary data analysis we studied the effects of several different buffer sizes, ranging from 500 meters to 9 km (the maximum distance recommended by EPA, 1992b). We determined that relatively short buffers are most appropriate because the Caline model is most reliable close to nearby sources. In this paper, we use Caline in 500 meter and 3 km buffers. It should be noted that our Caline predictions only include air pollution due to road traffic and do not include contributions from point sources. Examples of Caline predictions at three AQS sites are provided in Figure 1.

3. Model and Estimation. The primary interest of the MESA Air study is prediction of long-term averages at subject homes, however several factors necessitate explicit modeling of the 2-week average spatio-temporal field.

First, due to the sampling scheme we only have long-term time series of measurements at a few locations; our other measurements are irregularly distributed in space and time. Since the data exhibit temporal structure that varies with location (see Figure 1), we need to take the full spatio-

temporal structure of the data into account when combining measurements from different locations and times.

Second, modeling 2-week averages allows us to construct long-term averages over arbitrary time periods at each location. This makes it possible to calculate exposure based on any hypothesized timescale and to calculate total exposure over the entire study period for participants who have moved within our study area.

We let $C(s,t)$ denote the observed 2-week average concentration of NO_x at location s and time t, where s is a location index taking values in the set $\{1,\ldots,n\}$ and t is in $\{1,\ldots,T\}$. We let N denote the total number of observations and note that, due to our unbalanced sampling, $N \ll nT$. Our goal is to predict concentrations at locations and/or times that were not monitored. We denote these unknown values by $C^*(s,t)$. For convenience important notation is summarized in Table 3.

3.1. *Hierarchical model.* Denoting the logarithm of each two week average by $y(s,t)$, we decompose the field into

$$y(s,t) = \mu(s,t) + \nu(s,t). \tag{1}$$

Here $\mu(s,t)$ is the predictable mean field and $\nu(s,t)$ is the essentially random space-time residual field.

We model the mean field as

$$\mu(s,t) = \sum_{l=1}^{L} \gamma_l \mathcal{M}_l(s,t) + \sum_{i=1}^{m} \beta_i(s) f_i(t), \tag{2}$$

where the $\mathcal{M}_l(s,t)$ are spatio-temporal covariates with coefficients γ_l; $\{f_i(t)\}_{i=1}^m$ is a set of smooth basis functions, with $f_1(t) \equiv 1$ and $f_2(t),\ldots,f_m(t)$ having mean zero; and the $\beta_i(s)$ are spatially varying coefficients for the temporal trends. See Fuentes et al. (2006) and Szpiro et al. (2010a) for a similar mean field model without spatio-temporal covariates.

In this work we consider a single spatio-temporal covariate, the output from our Caline dispersion model. A possible interpretation of (2) is that we model the mean field as a simple scaling of the contribution from Caline, with a complex additive term that attempts to account for the spatial and temporal variations in air pollution that are not captured by Caline.

The complex additive term, $\sum_{i=1}^m \beta_i(s) f_i(t)$, is a linear combination of temporal basis functions weighted by coefficients that vary between locations. Typically the number of basis functions will be small. The basis functions are derived as smoothed singular vectors using observations from the

locations where we have nearly complete time series, i.e. most of the AQS sites; they will be treated as fixed and known for the modeling. Details can be found in Fuentes et al. (2006); Szpiro et al. (2010a); Sampson et al. (2009).

We model the spatial fields of β_i-coefficients using universal kriging (Cressie, 1993). The trend in the kriging is constructed as a linear regression on geographical covariates. The spatial dependence structure is provided by a set of covariance matrices $\Sigma_{\beta_i}(\theta_i)$, which are constructed from a known class of covariance functions and parameterized by unknown parameter vectors, θ_i. The resulting models for the β-fields are

$$\beta_i(s) \in \mathsf{N}\left(X_i\alpha_i, \Sigma_{\beta_i}(\theta_i)\right) \quad \text{for } i = 1, \ldots, m, \tag{3}$$

where X_i are $n \times p_i$ design matrices, α_i are $p_i \times 1$ matrices of regression coefficients, and $\Sigma_{\beta_i}(\theta_i)$ are $n \times n$ covariance matrices. Note that the design matrices, X_i, can incorporate different geographical covariates for the different spatial fields. We assume the $\beta_i(s)$ fields are independent of each other.

Finally, we must specify the model for the residual space-time field, $\nu(s,t)$. Following Sampson et al. (2009) and Szpiro et al. (2010a) we assume that the mean model, $\mu(s,t)$, accounts for the mean structure and most of the temporal correlation (see Figure 4). We model the residuals as a mean zero Gaussian field that is independent in time and has spatial dependence given by

$$\nu(s,t) \in \mathsf{N}\left(0, \Sigma_\nu^t(\theta_\nu)\right) \quad \text{for } t = 1, \ldots, T,$$

where the sizes of the covariance matrices, $\Sigma_\nu^t(\theta_\nu)$, are the numbers of observations, n_t, at each time-point. It should be noted that $\Sigma_\nu^t(\theta_\nu)$ does not imply a time varying covariance matrix; only the *number of elements* in $\Sigma_\nu^t(\theta_\nu)$ vary for different t. Elements in the covariance matrices are defined by assuming a known class of covariance functions that is parameterized by a set of unknown parameters, θ_ν.

We have assumed that the covariance matrices are constructed by plugging unknown parameters (which will have to be estimated) into a known class of covariance functions (e.g., one of those described in Cressie, 1993). It should be noted that there is nothing in the model that requires the different spatial fields to share a common covariance structure. This allows any non-stationarity in the space-time residuals to be accommodated using, e.g., deformation methods (Sampson, 2002; Damian et al., 2003), while retaining a stationary covariance structure for the β_i-fields.

Here we use exponential covariance functions, characterized by range ϕ, partial sill σ^2, and nugget τ^2. To obtain a smooth mean field in (2) we assume that the nuggets of the β_i-fields are zero. Thus, the parameters of the model consist of: the regression parameters for the geographical, and spatio-temporal covariates, respectively

$$\boldsymbol{\alpha} = (\alpha_1^\top, \ldots, \alpha_m^\top)^\top; \qquad \boldsymbol{\gamma} = (\gamma_1, \ldots, \gamma_L)^\top,$$

spatial covariance parameters for the β_i-fields,

$$\theta_B = (\theta_1, \ldots, \theta_m) \quad \text{where} \quad \theta_i = (\phi_i, \sigma_i^2),$$

and covariance parameters of the spatio-temporal residuals,

$$\theta_\nu = (\phi_\nu, \sigma_\nu^2, \tau_\nu^2).$$

To simplify notation we collect the covariance parameters into Ψ,

$$\Psi = (\theta_1, \ldots, \theta_m, \theta_\nu).$$

Combining (1) and (2) our model becomes

$$y(s,t) = \sum_{l=1}^{L} \gamma_l \mathcal{M}_l(s,t) + \sum_{i=1}^{m} \beta_i(s) f_i(t) + \nu(s,t). \tag{4}$$

Following Szpiro et al. (2010a), we introduce the $N \times 1$-vectors $Y = y(s,t)$ and $V = \nu(s,t)$ by stacking the elements into single vectors varying first s and then t; a $mn \times 1$-vector $B = (\beta_1(s)^\top, \ldots, \beta_m(s)^\top)^\top$; and a sparse $N \times mn$-matrix $F = (f_{st,is'})$ with elements

$$f_{st,is'} = \begin{cases} f_i(t) & s = s' \\ 0 & \text{otherwise.} \end{cases}$$

To accommodate the spatio-temporal covariates we also introduce a $N \times L$-matrix $\mathcal{M}$, with each row containing covariates for the space-time location of the corresponding row in Y.

Using these matrices we rewrite (4) as

$$Y = \mathcal{M}\boldsymbol{\gamma} + FB + V, \tag{5}$$

where

$$B \in \mathsf{N}\left(X\boldsymbol{\alpha}, \Sigma_B(\theta_B)\right) \quad \text{and} \quad V \in \mathsf{N}\left(0, \Sigma_\nu(\theta_\nu)\right).$$

Here X, $\Sigma_B(\theta_B)$, and $\Sigma_\nu(\theta_\nu)$ are block diagonal matrices with diagonal blocks $\{X_i\}_{i=1}^m$, $\{\Sigma_{\beta_i}(\theta_i)\}_{i=1}^m$, and $\{\Sigma_\nu^t(\theta_\nu)\}_{t=1}^T$ respectively. Noting that (5) is a linear combinations of Gaussians we introduce the matrices

$$\widetilde{X} = \begin{bmatrix} \mathcal{M} & FX \end{bmatrix} \quad \text{and} \quad \widetilde{\Sigma}(\Psi) = \Sigma_\nu(\theta_\nu) + F\Sigma_B(\theta_B)F^\top,$$

and write the distribution of Y as

$$[Y|\Psi, \boldsymbol{\gamma}, \boldsymbol{\alpha}] \in \mathsf{N}\left(\widetilde{X}\begin{bmatrix}\boldsymbol{\gamma}\\ \boldsymbol{\alpha}\end{bmatrix}, \widetilde{\Sigma}(\Psi)\right). \tag{6}$$

Estimating the unknown parameters, $(\Psi, \boldsymbol{\gamma}, \boldsymbol{\alpha})$, can now be accomplished by maximizing the log-likelihood

$$\begin{aligned} 2l(\Psi, \boldsymbol{\gamma}, \boldsymbol{\alpha}|Y) = &- N\log(2\pi) - \log\left|\widetilde{\Sigma}(\Psi)\right| \\ &- \left(Y - \widetilde{X}\begin{bmatrix}\boldsymbol{\gamma}\\ \boldsymbol{\alpha}\end{bmatrix}\right)^\top \widetilde{\Sigma}^{-1}(\Psi)\left(Y - \widetilde{X}\begin{bmatrix}\boldsymbol{\gamma}\\ \boldsymbol{\alpha}\end{bmatrix}\right). \end{aligned} \tag{7}$$

3.2. *Parameter estimation.* Given the large monitoring database, estimating parameters by naïve maximum likelihood (ML) takes considerable computer time. There are two considerations of importance for minimizing the required computer time: 1) reducing the number of parameters should speed up the estimation, and 2) the block structure of $\Sigma_\nu(\theta_\nu)$ and $\Sigma_B(\theta_B)$ can be exploited to reduce the computational burden of evaluating the log-likelihood.

It is trivial to show that the generalized least-squares fit

$$\begin{bmatrix}\boldsymbol{\gamma}(\Psi)\\ \boldsymbol{\alpha}(\Psi)\end{bmatrix} = \left(\widetilde{X}^\top\widetilde{\Sigma}^{-1}(\Psi)\widetilde{X}\right)^{-1}\widetilde{X}^\top\widetilde{\Sigma}^{-1}(\Psi)Y \tag{8}$$

maximizes the log-likelihood with respect to $\boldsymbol{\gamma}$ and $\boldsymbol{\alpha}$, for any values of Ψ. Replacing $\boldsymbol{\gamma}$ and $\boldsymbol{\alpha}$ with the functions of Ψ obtained in (8) reduces the unknown parameters in the log-likelihood to only Ψ. This corresponds to the profile log-likelihood which, after some algebra, is

$$\begin{aligned} 2l_{\text{PROF}}(\Psi|Y) = &- N\log(2\pi) - \log\left|\widetilde{\Sigma}(\Psi)\right| - Y^\top\widetilde{\Sigma}^{-1}(\Psi)Y \\ &+ Y^\top\widetilde{\Sigma}^{-1}(\Psi)\widetilde{X}\left(\widetilde{X}^\top\widetilde{\Sigma}^{-1}(\Psi)\widetilde{X}\right)^{-1}\widetilde{X}^\top\widetilde{\Sigma}^{-1}(\Psi)Y. \end{aligned} \tag{9}$$

Note that the value Ψ that maximizes the profile likelihood also maximizes the original likelihood (7).

The profile likelihood reduces the number of unknown parameters but it does not utilize the block structure of $\Sigma_\nu(\theta_\nu)$ and $\Sigma_B(\theta_B)$. A way of rewriting (9) that utilizes the structure to significantly reduce the computational burden is provided in Appendix A. As an example, evaluating the likelihood *once* for our 5181 measurements in Los Angeles takes 92 seconds using the original profile likelihood formulation (9), compared to 2.5 seconds after simplifications (on an Intel Xeon E5410 processor). Figure 5 provides comparisons of evaluation times for different size datasets. Both the faster evaluation time for the optimized likelihood, as well as the much slower increase in computation time as a function of dataset size, both in terms of number of observations and number of spatial locations, are illustrated. Additional theoretical details regarding the computational burden can be found in Appendix A.2.

We use the constrained L-BFGS-B algorithm implemented in the `optim()` function in R (Byrd et al., 1995; R Development Core Team, 2008) to optimize the profile likelihood, first log-transforming the covariance parameters to make the optimization easier. We denote the estimated parameters by $\widehat{\Psi}_{\text{PROF}}$, $\widehat{\boldsymbol{\gamma}}_{\text{PROF}}$, and $\widehat{\boldsymbol{\alpha}}_{\text{PROF}}$. To obtain approximate uncertainties for the estimated parameters we compute the finite difference Hessian of the full log-likelihood and take the negative diagonal elements of its inverse (i.e., we use the observed information matrix).

3.2.1. *Restricted Maximum Likelihood.* An alternative option for reducing the number of parameters is restricted maximum likelihood (REML) (Patterson and Thompson, 1971; Harville, 1974). In classical statistical terms, the principal difference between profile likelihood (equivalently ML) and REML is that REML accounts for the loss in the degrees of freedom associated with estimation of the regression parameters, $\boldsymbol{\gamma}$ and $\boldsymbol{\alpha}$, when estimating the covariance. A Bayesian interpretation is that REML assumes flat priors and marginalizes the full likelihood with respect to $\boldsymbol{\gamma}$ and $\boldsymbol{\alpha}$ (see Harville, 1974, for details).

Simulation studies indicate that REML estimates of variance parameters are less biased than ML estimates (Swallow and Monahan, 1984; Cressie and Lahiri, 1993). However, due to the bias-variance trade-off, ML estimates can exhibit smaller mean squared errors than REML estimates for some models (Swallow and Monahan, 1984). Further, the magnitude of the bias in ML depends on the number of regression parameters compared to the number of observations and decreases with increasing sample size. In this study we use the profile likelihood, but for completeness parallel results for REML are given in Appendix B.

The primary reason we prefer profile likelihood is that it is equivalent to ML, and our predictions will be used as exposures in a health effects model where it is natural to account for the joint variability of all the estimated exposure model parameters using the full likelihood (Szpiro et al., 2010b). Also, in a simple simulation study based on parts of our data we found a small bias reduction from using REML, but the numerical estimation for REML was significantly more time consuming and prone to non-convergence.

3.3. *Prediction.* Having obtained values for the parameters the next step is to predict concentrations at unobserved locations and times. As previously noted we let $C^*(s,t)$ denote these unobserved values. By adding the unobserved times and locations to our model we expand the distribution in (6) to include $y^*(s,t) = \log C^*(s,t)$, or

$$\begin{bmatrix} Y \\ Y^* \end{bmatrix} \Big| \Psi, \boldsymbol{\gamma}, \boldsymbol{\alpha} \Bigg] \in \mathsf{N}\left(\begin{bmatrix} \widetilde{X} \\ \widetilde{X}^* \end{bmatrix} \begin{bmatrix} \boldsymbol{\gamma} \\ \boldsymbol{\alpha} \end{bmatrix}, \begin{bmatrix} \widetilde{\Sigma}_{..}(\Psi) & \widetilde{\Sigma}_{.*}(\Psi) \\ \widetilde{\Sigma}_{.*}^{\top}(\Psi) & \widetilde{\Sigma}_{**}(\Psi) \end{bmatrix} \right), \tag{10}$$

where $\widetilde{\Sigma}_{..}$ is the covariance matrix for the observed data, $\widetilde{\Sigma}_{**}$ is the covariance for the unobserved data, and $\widetilde{\Sigma}_{.*}$ is the cross-covariance between observed and unobserved data. Finally $\widetilde{X}^*$ is constructed using the spatio temporal covariates, temporal trends, and geographical covariates for the unobserved data.

Predictions and prediction uncertainties are obtained as the conditional expectation and conditional variance of (10). The prediction variance is

$$\mathsf{V}\big(Y^* \big| Y, \widehat{\Psi}_{\text{PROF}}, \widehat{\boldsymbol{\gamma}}_{\text{PROF}}, \widehat{\boldsymbol{\alpha}}_{\text{PROF}}, \big) = \widetilde{\Sigma}_{**} - \widetilde{\Sigma}_{.*}^{\top} \widetilde{\Sigma}_{..}^{-1} \widetilde{\Sigma}_{.*} \tag{11}$$

where all the covariance matrices are evaluated at $\widehat{\Psi}_{\text{PROF}}$.

The approximate parameter uncertainties are computed using the observed information matrix and are based on asymptotic maximum likelihood theory (see, e.g. Casella and Berger, 2002); the prediction uncertainties (11) do not account for uncertainties in the estimated parameters. One option for obtaining full prediction uncertainties is to use Markov Chain Monte Carlo (MCMC) (Metropolis et al., 1953; Hastings, 1970) or some other numerical integration scheme (Rue et al., 2009). An appealing option when using MCMC is to first maximize the likelihood using numerical optimization and then use the observed information matrix to construct a Metropolis-random-walk-algorithm with optimal proposal distribution (Gelman et al., 1996). This approach is implemented in our R package, `SpatioTemporal`. Using MCMC, however, adds considerable computer time and is not feasible for our cross-validation study.

3.4. *Validation.* We use cross-validation to assess the predictive accuracy of our model. Our primary interest is the prediction of long-term averages, but we have only 25 monitors (AQS and MESA fixed sites) that provide time series against which we can validate predictions of long-term averages. Due to AQS siting, these 25 monitors have less heterogeneity in their geographic covariates but larger spatial spread when compared to participant home locations, potentially limiting our ability to correctly assess model performance.

To make the fullest use of available data we employ three different cross-validation strategies: 1) leave-one-out cross-validation for the AQS and MESA fixed sites (the two colocated sites are kept together, resulting in 24 groups), 2) 10-fold cross-validation for the sites in the snapshot campaign (ensuring not to split road gradients between groups); and 3) 10-fold cross-validation of the home outdoor sites. For each of the scenarios above, all remaining data are used to estimate parameters and to predict at the left out locations. Given the predictions and prediction variances (11) we compute the coverage for 95% prediction intervals, the root mean squared error (RMSE) and the corresponding cross-validated R^2.

For the first cross-validation approach we validate the model by comparing predicted and observed 2-week averages, as well as the predicted and observed long-term average concentration at each location. To compute the true long-term averages we use time points for which we have observations at that location, and we compute predicted long-term averages using the predicted 2-week average concentrations at the corresponding times,

$$C^*(s) = \sum_{t \in \{\tau\,:\,\exists y(s,\tau)\}} \frac{\exp(y^*(s,t))}{\|\{\tau\,:\,\exists y(s,\tau)\}\|}.$$

The cross-validated R^2 are computed as

$$R^2 = \max\left(0, 1 - \frac{\mathrm{RMSE}^2}{\mathrm{Var}(C(s))}\right).$$

For the MESA Air snapshot campaign, we calculate cross-validated predictions by simultaneously leaving out measurements in the validation set for all three seasons. However, when assessing the spatial predictive ability of our model, we compute separate RMSE and R^2 values for each season. This has the added benefit of providing information regarding the model's differential spatial predictive ability in each season.

For the MESA Air home campaign the situation is slightly more complicated since our measurements are spread out in time and space. We compute

the RMSE value as usual, but for R^2 we compare our predictions to a simple reference model that accounts for the temporal variability. We use the formula

$$R^2 = \max\left(0, 1 - \frac{\text{RMSE}^2}{\text{RMSE}^2_{\text{ref}}}\right),$$

where $\text{RMSE}^2_{\text{ref}}$ denotes the RMSE of a reference model to which we compare our predictions. Reference models used are: 1) the spatial average at each time point based on observations at AQS and MESA fixed sites; 2) the closest available observation from the AQS and MESA fixed sites; 3) smooth temporal trends fitted to the data at the closest AQS or MESA fixed sites. These three reference models will be denoted as *average*, *closest*, and *smooth* in the rest of this document. This R^2 can also be seen as the improvement in prediction provided by our model when compared to the use of the central site or nearest neighbor schemes common in published epidemiology studies (Pope et al., 1995; Goss et al., 2004; Miller et al., 2007).

4. Different ways of including Caline. We have considered several different options for including the Caline predictions in the spatio-temporal model. Because our observations are log-transformed, a similar transformation of Caline seems reasonable. However, since the Caline predictions include contribution from major roads within the 500m or 3km buffers, we use a $\log(x+1)$ transformation to accommodate zeros. Preliminary studies with no transformation, or including first, second, and third order terms to account for potential non-linearities indicated results similar to, or worse than, the $\log(x+1)$ transformation.

A second issue is that the unbalanced monitoring scheme, with long-time series at a few sites, may cause the model fit to emphasize Caline's temporal predictive ability over its spatial features. Therefore, we also consider the performance of a mean separated Caline variable. For the mean separated Caline, we take $\mathcal{M}(s,t) = \log(\text{Caline}+1)$, compute the temporal average at each location

$$\overline{\mathcal{M}}(s) = \frac{1}{T}\sum_t \mathcal{M}(s,t),$$

and calculate a new spatio-temporal covariate that is mean-zero at each site

$$\widetilde{\mathcal{M}}(s,t) = \mathcal{M}(s,t) - \overline{\mathcal{M}}(s).$$

The average, $\overline{\mathcal{M}}(s)$, is added to the list of geographic covariates and $\widetilde{\mathcal{M}}(s,t)$ is used as a spatio-temporal covariate, allowing us to separate Caline's spatial and temporal contributions to the predictions.

5. Results.

5.1. *Geographic covariate predictors only (no Caline).* Cross-validation results for the model with only geographic covariates (no Caline) are presented in Table 4. Figure 6 shows the cross-validated predictions, along with observed data and prediction intervals at three AQS sites, and Figure 7 shows predictions of long-term averages at the AQS and MESA fixed sites. The estimated parameters for the model fit to all the data are given in Table 7.

The predictive ability at MESA home sites is very good, with $R^2 \approx 0.9$. Even after the use of a simple reference model to account for the temporal variability, the spatial predictive ability remains high, with $R^2 \approx 0.67 - 0.74$ depending on the reference model used. The R^2 values are slightly lower for the summer snapshot ($R^2 \approx 0.52$) and long-term averages ($R^2 \approx 0.58$). The lowest RMSE values are also found during the summer snapshot, indicating that there is little variability to explain in this dataset. The lower R^2 values for the long-term averages are also expected because many AQS sites are either far from other sites or at the edge of our area of interest (see the map in Figure 2). Due to the spatial dependence in our model, we expect cross-validation at these sites to exhibit larger prediction errors than at subject home locations. Our uncertainty estimates are also reasonable, with the coverage for 95% prediction intervals varying from 91% to 99% for all three cross-validation approaches.

5.2. *Geographic covariates and Caline predictors.* Our primary implementation of Caline is mean separated with a 3 km buffer. Results for the version that is not mean separated and for a 500 meter buffer are similar or slightly worse (see Table 5). The estimated parameters for the model with and without Caline are compared in Table 7. It is worth noting that the estimated coefficient for the contribution from the time averaged Caline to the spatial intercept (the Caline coefficient in β_1) is statistically significant as is the contribution from the spatio temporally varying Caline (the γ-coefficient). Several of the regression coefficients for the temporal trends (β_2 and β_3) are not significant, however attempts to reduce the number of covariates for the β_2 and β_3 fields decreased the cross-validated performance. Coefficients for the other geographic covariates are very similar in the model with and without Caline. Cross-validation results for the model with Caline are given in Table 4. For this implementation there is no evidence of improved performance compared to the model without Caline.

One possible explanation for the lack of improvement from Caline is that the model already contains road covariates that are good predictors of traffic

related NO_x. In an attempt to compare the predictive ability of road covariates with that of Caline, we fit the model again without any of the GIS road covariates, with and without Caline. Estimated parameters for both models are presented in Table 8. The estimated parameters for the two β-fields that affect the temporal trends are very similar, indicating that the variation in temporal trends over the region is not primarily driven by local road/traffic effects. For the long-term average β_1-field there are differences in estimated parameters. The effect of population density is almost halved when Caline is included, and the estimated range parameter for β_1 is only 530 m without Caline, compared to 3.7 km when including Caline. The coefficient for Caline in the β_1-field is much larger than in the model with road covariates (0.145 compared to 0.0789), indicating that without the road covariates the contribution from Caline is more important.

Cross-validation results are presented in Table 6 and Figure 7. Without the road covariates in the model, including Caline results in uniformly better cross-validation results than for the model without Caline. In fact, predictions with this model are nearly comparable to those obtained from the model that includes road covariates but not Caline. This suggests that our implementation of Caline may be able to provide interpretable replacement for GIS road covariates, even though it does not provide additional predictive power in a model that already includes roadway information.

6. Discussion. In this paper we have expanded the spatio-temporal framework introduced by (Sampson et al., 2009; Szpiro et al., 2010b) to allow for spatio-temporally varying covariates. The resulting model provides a flexible way of combining observations with the output from deterministic air quality models. The model presented in this paper has been implemented in an R-package, `SpatioTemporal` that will be available on CRAN shortly.

To make the model computationally feasible, we used profile likelihood (and REML) to reduce the number of parameters that have to be estimated. Further, the structure in the model, with spatially correlated but temporally independent residuals, allowed us to rewrite the likelihood into a computationally efficient form. The importance of these simplifications cannot be stressed enough, as they reduce the computational burden by more than an order of magnitude.

The model was applied to the full MESA Air dataset in Los Angeles, and a thorough cross-validation study was done to evaluate prediction performance. In order for us to make the fullest use of the unbalanced monitoring in the MESA Air study, special care was taken when designing the cross-validation study in order to focus on predicting long-term averages,

even though much of our validation data are collected over short time periods. The cross-validation study shows good predictive power, especially at subject home locations. This indicates that our spatio-temporal model will be able to provide the basis for high quality predicted exposures in our health analysis. Furthermore, our profile likelihood estimation methodology provides uncertainty estimates suitable for use in our recently developed methods to adjust for measurement error that results from using predicted exposures in place of the true values (Szpiro et al., 2010b).

Including Caline as an additional predictor variable provided essentially no overall improvement in prediction accuracy. This came as somewhat of a surprise to the authors, especially since a previous pilot study (Wilton et al., 2010) indicated improved prediction performance for the summer snapshot. However, consistent with the pilot study, we find some improvement for the summer snapshot when including Caline (see Table 4). One reason for this lack of improvement may be that we used a constant unit emissions fatcor that does not account for changes to the fleet over time. As future research we will weight our Caline predictions by including trends in fleet emissions (by e.g. using the EPA's MOVES model; EPA, 1992a). Our results do, however, suggest that Caline may provide a more directly interpretable replacement for GIS road covariates, potentially limiting the need for model selection from multiple road covariates corresponding to different road classes and buffer sizes.

Our results contrast with other studies that have shown improvement in air quality predictions by combining observations with output from deterministic models (e.g. Fuentes and Raftery, 2005; Berrocal et al., 2010; McMillan et al., 2010). These studies do not use any GIS covariates, but do use output from grid based models over large geographic areas, often several states. These differences make it difficult to translate their results to our limited geographic areas and study design. Given the relatively compact geographical areas in the MESA Air study and our need to resolve small-scale spatial variability, the potential gain from grid based models is limited. The most commonly used model, EPA's Community Multiscale Air Quality (CMAQ), produces predictions on 4, 12, or 36 km grids (most typically 12 km). With a 12 km grid our Los Angeles study area can be covered using only 30 grid cells, so a grid-based model of this resolution would provide limited spatial information over our study area.

Acknowledgments. Although the research described in this article has been funded wholly or in part by the United States Environmental Protection Agency through assistance agreement CR-834077101-0 and grant

RD831697 to the University of Washington, it has not been subjected to the Agency's required peer and policy review and therefore does not necessarily reflect the views of the Agency and no official endorsement should be inferred.

Travel for Johan Lindström has been paid by STINT (The Swedish Foundation for International Cooperation in Research and Higher Education) Grant IG2005-2047.

Additional funding was provided by grants to the University of Washington from the Health Effects Institute (4749-RFA05-1A/06-10) and the National Institute of Environmental Health Sciences (P50 ES015915).

The MESA cohort study is supported by contracts N01-HC-95159 through N01-HC-95169 from the National Heart, Lung, and Blood Institute. The authors thank the other investigators, the staff, and the participants of the MESA study for their valuable contributions. A full list of participating MESA investigators and institutions can be found at `http://www.mesa-nhlbi.org`.

References.

Appel, K. W., Bhave, P. V., Gilliland, A. B., Sarwar, G. and Roselle, S. J. (2008). Evaluation of the community multiscale air quality (CMAQ) model version 4.5: Sensitivities impacting model performance; part II-particulate matter. *Atmo. Environ.*, **42** 6057–6066.

Banerjee, S., Carlin, B. P. and Gelfand, A. E. (2004). *Hierarchical Modeling and Analysis for Spatial Data*. Chapman and Hall, CRC.

Basu, R., Woodruff, T. J., Parker, J. D., Saulnier, L. and Schoendorf, K. C. (2000). Particulate air pollution and mortality: Findings from 20 U.S. cities. *N. Engl. J. Med.*, **343** 1742–1749.

Berrocal, V. J., Gelfand, A. E. and Holland, D. M. (2010). A spatio-temporal downscaler for output from numerical models. *J. Agric. Bio. and Environ. Statist.*

Bild, D. E., Bluemke, D. A., Burke, G. L., R., D., Diez Roux, A. V., Folsom, A. R., Greenland, P., Jacob, D. R., Jr, Kronmal, R., Liu, K., Nelson, J. C., O'Leary, D., Saad, M. F., Shea, S., Szklo, M. and Tracy, R. P. (2002). Multi-ethnic study of atherosclerosis: Objectives and design. *American Journal of Epidemiology*, **156** 871–881.

Brauer, M., Hoek, G., van Vliet, P., Meliefste, K., Fischer, P., Gehring, U., Heinrich, J., Cyrys, J., Bellander, T., Lewne, M. and Brunekreef, B. (2003). Estimating long-term average particulate air pollution concentrations: Application of traffic indicators and geographic information systems. *Epidemiology*, **14** 228–239.

Byrd, R., Lu, P., Nocedal, J. and Zhu, C. (1995). A limited memory algorithm for bound constrained optimization. *SIAM J. Sci. Comput.* 1190–1208.

Carroll, R. J., Ruppert, D., Stefanski, L. A. and Crainiceanu, C. M. (2006). *Measurement Error in Nonlinear Models: A Modern Perspective*. 2nd ed. Chapman and Hall, CRC.

Casella, G. and Berger, R. L. (2002). *Statistical Inference*. 2nd ed. Duxbury.

Cohen, M. A., Adar, S. D., Allen, R. W., Avol, E., Curl, C. L., Gould, T., Hardie, D., Ho, A., Kinney, P., Larson, T. V., Sampson, P. D., Sheppard, L., Stukovsky,

K. D., Swan, S. S., Liu, L.-J. S. and Kaufman, J. D. (2009). Approach to estimating participant pollutant exposures in the Multi-Ethnic Study of Atherosclerosis and air pollution (MESA air). *Environ. Sci. Technol.*, **43** 4687–4693.

Cressie, N. (1993). *Statistics for Spatial Data*. Revised ed. John Wiley & Sons Ltd.

Cressie, N. and Lahiri, S. (1993). The asymptotic distribution of reml estimators. *Journal of Multivariate Analysis*, **45** 217–233.

Damian, D., Sampson, P. D. and Guttorp, P. (2003). Variance modeling for nonstationary processes with temporal replications. *J. Geophys. Res.*, **108** 8778.

Dockery, D. W., Pope, C. A., Xu, X., Spangler, J. D., Ware, J. H., Fay, M. E., Ferris, B. G. and Speizer, F. E. (1993). An association between air pollution and mortality in six cities. *N. Engl. J. Med.*, **329** 1753–1759.

EPA (1992a). Technical guidance on the use of MOVES2010 for emission inventory preparationin state implementation plans and transportation conformity. Tech. Rep. EPA-420-B-10-023, U.S. Environmental Protection Agency.

EPA (1992b). User's guide to CAL3QHC version 2.0: A modeling methodology for predicting pollutant concentrations near roadway intersections. Tech. Rep. EPA-454/R-92-006, U.S. Environmental Protection Agency, Research Triangle Park, NC, USA.

Fanshawe, T. R., Diggle, P. J., Rushton, S., Sanderson, R., Lurz, P. W. W., Glinianaia, S. V., Pearce, M. S., Parker, L., Charlton, M. and Pless-Mulloli, T. (2008). Modelling spatio-temporal variation in exposure to particulate matter: a two-stage approach. *Environmetrics*, **19** 549–566.

Fuentes, M., Guttorp, P. and Sampson, P. D. (2006). Using transforms to analyze space-time processes. In *Statistical Methods for Spatio-Temporal Systems* (B. Finkenstadt, L. Held and V. Isham, eds.). CRC/Chapman and Hall, 77–150.

Fuentes, M. and Raftery, A. E. (2005). Model evaluation and spatial interpolation by Bayesian combination of observations with outputs from numerical models. *Biometrics*, **61** 34–45.

Gelman, A., Roberts, G. and Gilks, W. (1996). Efficient metropolis jumping rules. In *Bayesian Statistics 5* (J. M. Bernardo, J. O. Berger, A. P. Dawid and A. F. M. Smith, eds.). Oxford University Press, 599–607.

Goss, C. H., Newsom, S. A., Schildcrout, J. S., Sheppard, L. and Kaufman, J. D. (2004). Effect of ambient air pollution on pulmonary exacerbations and lung function in cystic fibrosis. *Am. J. Respir. Crit. Care med.*, **169** 816–821.

Gotway, C. and Young, L. (2002). Combining incompatible spatial data. *J. Amer. Statist. Assoc.*, **97** 632–648.

Gryparis, A., Paciorek, C. J., Zeka, A., Schwartz, J. and Coull, B. A. (2009). Measurement error caused by spatial misalignment in environmental epidemiology. *Biostatistics*, **10** 258–274.

Harville, D. A. (1974). Bayesian inference for variance components using only error contrasts. *Biometrika*, **61** 383–385.

Harville, D. A. (1997). *Matrix Algebra From a Statistician's Perspective*. 1st ed. Springer.

Hastings, W. (1970). Monte Carlo sampling methods using Markov chains and their applications. *Biometrika*, **57** 97–109.

Hoek, G., Beelena, R., de Hoogh, K., Vienneaub, D., Gulliverc, J., Fischer, P. and Briggs, D. (2008). A review of land-use regression models to assess spatial variation of outdoor air pollution. *Atmo. Environ.*, **42** 7561–7578.

Hogrefe, C., Porter, P., Gego, E., Gilliland, A., Gilliam, R., Swall, J., Irwin, J. and Rao, S. (2006). Temporal features in observed and simulated meteorology and air quality over the eastern united states. *Atmo. Environ.*, **40** 5041–5055.

Irwin, J. S. (2002). *A historical look at the development of regulatory air quality models for the United States Environmental Protection Agency*, vol. 244 of *NOAA technical memorandum OAR ARL*. U.S. Dept. of Commerce, National Oceanic and Atmospheric Administration.

Jerrett, M., Arain, A., Kanaroglou, P., Beckerman, B., Potoglou, D., Sahsuvaroglu, T., Morrison, J. and Giovis, C. (2005a). A review and evaluation of intraurban air pollution exposure models. *J. Exposure Anal. Environ. Epidemiol.*, **15** 185–204.

Jerrett, M., Burnett, R. T., Ma, R., Pope, C. A., Krewski, D., Newbold, K. B., Thurston, G., Shi, Y., Finkelstein, N., Calle, E. E. and Thun, M. J. (2005b). Spatial analysis of air pollution mortality in Los Angeles. *Epidemiology*, **16** 727–736.

Kunzli, N., Jerrett, M., Mack, W. J., Beckerman, B., LaBree, L., Gilliland, F., Thomas, D., Peters, J. and Hodis, H. N. (2005). Ambient air pollution and atherosclerosis in Los Angeles. *Environ. Health Persp.*, **113** 201–206.

Lindström, J., Sampson, P. D., Guttorp, P. and Sheppard, L. (2010). Spurious correlations; potential pitfalls when evaluating air quality models against observations. *In preparation*.

Mathur, R., Yu, S., Kang, D. and Schere, K. L. (2008). Assessment of the wintertime performance of developmental particulate matter forecasts with the EPA-Community Multiscale Air Quality modeling system. *J. Geophys. Res.*, **113** D02303.

McMillan, N. J., Holland, D. M., Morara, M. and Feng, J. (2010). Combining numerical model output and particulate data using bayesian space-time modeling. *Environmetrics*, **21** 48–65.

Mercer, L., Szpiro, A. A., Sheppard, L., Adar, S., Allen, R., Avol, E., Lindström, J., Oron, A., Larson, T., Liu, L.-J. S. and Kaufman, J. (2010). Predicting concentrations of oxides of nitrogen in Los Angeles, CA using universal kriging. *TBD*, **?** Work in progress.

MESA Air Data Team (2010). Documentation of MESA air implementation of the Caline3QHCR model. Tech. rep., University of Washington, Seattle, WA, USA.

Metropolis, N., Rosenbluth, A., Rosenbluth, M., Teller, A. and Teller, E. (1953). Equations of state calculations by fast computing machines. *J. Chem. Phys.*, **21** 1087–1092.

Miller, K. A., Sicovick, D. S., Sheppard, L., Shepherd, K., Sullivan, J. H., Anderson, G. L. and Kaufman, J. D. (2007). Long-term exposure to air pollution and incidence of cardiovascular events in women. *N. Engl. J. Med.*, **356** 447–458.

Paciorek, C. P., Yanosky, J. D., Puett, R. C., Laden, F. and Suh, H. H. (2009). Practical large-scale spatio-temporal moeling of particulate matter concentrations. *Ann. Statist.*, **3** 370–397.

Patterson, H. D. and Thompson, R. (1971). Recovery of inter-block information when block sizes are unequal. *Biometrika*, **58** 545–554.

Pope, C. A., Burnett, R. T., Thun, M. J., Calle, E. E., Krewski, D., Ito, K. and Thurston, G. D. (2002). Lung cancer, cardiopulmonary mortality, and long-term exposure to fine particulate air pollution. *J. Am. Med. Assoc.*, **9** 1132–1141.

Pope, C. A., Thun, M. J., Namboodiri, M. M., Dockery, D. W., Evans, J. S., Speizer, F. E. and Heath, C. W., Jr. (1995). Particulate air pollution as a predictor of mortality in a prospective study of U.S. adults. *Am. J. Respir. Crit. Care med.*, **151** 669–674.

Puett, R. C., Hart, J. E., Yanosky, J. D., Paciorek, C. J., Schwartz, J., Suh, H., Speizer, F. E. and Laden, F. (2009). Chronic fine and coarse particulate exposure, mortality and coronary heart disease in the nurses' health study. *Environ. Health Persp.*,

117 1697–1701.

R Development Core Team (2008). *R: A Language and Environment for Statistical Computing*. R Foundation for Statistical Computing, Vienna, Austria. ISBN 3-900051-07-0, URL `http://www.R-project.org`.

Ritz, B., Wilhelm, M. and Zhao, Y. (2006). Air pollution and infant death in southern California, 1989-2000. *Pediatrics*, **118** 493–502.

Rue, H., Martino, S. and Chopin, N. (2009). Approximate Bayesian inference for hierarchical Gaussian Markov random field models. *J. Roy. Statist. Soc. Ser. B*, **71** 1–35.

Sahu, S. K., Gelfand, A. E. and Holland, D. (2006). Spatio-temporal modeling of fine particulate matter. *J. Agric. Bio. and Environ. Statist.*, **11** 61–86.

Sampson, P. D. (2002). Spatial covariance. In *Encyclopedia of Environmetrics* (A. El-Shaarawi and W. W. Pierorcsh, eds.), vol. 4. Wiley, 2059–2067.

Sampson, P. D., Szpiro, A. A., Sheppard, L., Lindström, J. and Kaufman, J. D. (2009). Pragmatic estimation of a spatio-temporal air quality model with irregular monitoring data. Tech. Rep. Working Paper 353, UW Biostatistics Working Paper Series. URL `http://www.bepress.com/uwbiostat/paper353`.

Smith, R. L., Kolenikov, S. and Cox, L. H. (2003). Spatio-temporal modeling of PM2.5 data with missing values. *J. Geophys. Res.*, **108** 9004.

Swallow, W. H. and Monahan, J. F. (1984). Monte carlo comparison of ANOVA, MIVQUE, REML, and ML estimators of variance components. *Technometrics*, **26** 47–57.

Szpiro, A. A., Sampson, P. D., Sheppard, L., Lumley, T., Adar, S. and Kaufman, J. (2010a). Predicting intra-urban variation in air pollution concentrations with complex spatio-temporal dependencies. *Environmetrics*, **21** 606–631.

Szpiro, A. A., Sheppard, L. and Lumley, T. (2010b). Efficient measurement error correction with spatially misaligned data. Tech. Rep. Working Paper 350, UW Biostatistics Working Paper Series. URL `http://www.bepress.com/uwbiostat/paper350`.

Wilton, D., Szpiro, A. A., Gould, T. and Larson, T. (2010). Improving spatial concentration estimates for nitrogen oxides using a hybrid meteorological dispersion/land use regression model in Los Angeles, CA and Seattle, WA. *Sci. Total Environ.*, **408** 1120–1130.

Table 1
Summary of observations used for modeling

Type of site	Nbr. of sites	Start date	End date	Nbr. of measurement
AQS	20	1999–01–13	2009–09–23	4178
MESA fixed	5	2005–12–07	2009-07-01	399
MESA home	84	2006–05–24	2008–02–13	155
MESA snapshot[1]	177	2006–07–05	2007–01–31	449

[1]Snapshot measurements where carried out during three 2-week periods centered on the Wednesdays of 2006–07–05, 2006–10–25, and 2007–01–31

TABLE 2
Summary statistics for the data, both on the original ppb scale and on the log-scale.

	ppb NO_x		log(ppb NO_x)	
	Mean	Std.	Mean	Std.
AQS and MESA fixed				
2-week	55.5	39.9	3.77	0.724
long-term avg.	56.0	18.4	3.77	0.394
Snapshot				
2006–07–05	34.2	11.5	3.47	0.387
2006–10–25	75.1	23.5	4.27	0.317
2007–01–31	95.3	27.0	4.51	0.299
Home sites	45.6	28.3	3.63	0.642

TABLE 3
Important notation and symbols

Symbol	Meaning
$C(s,t)$	Observed 2-week average concentration.
$C^*(s,t)$	Unobserved 2-week average concentration.
$y(s,t)$	The logarithm of $C(s,t)$.
$y^*(s,t)$	The logarithm of $C^*(s,t)$.
$\mu(s,t)$	Predictable mean field part of $y(s,t)$.
$\nu(s,t)$	Space-time residual part of $y(s,t)$.
$f_i(t)$	Smooth temporal basis functions.
$\beta_i(s)$	Spatially varying regression coefficients, weighing the i:th temporal trends differently at each site.
X_i	Land use regression (LUR) basis functions for the spatially varying regression coefficients in $\beta_i(s)$.
α_i	Regression coefficients for the i:th LUR-basis.
$\mathcal{M}_l(s,t)$	Spatio-temporally varying covariates.
γ_l	Regression coefficient for the spatio-temporally varying covariates.
N	Total number of observations.
T	Total number of observed time-points.
n	Total number of observed sites.
n_t	Number of observations at time t. Note that $N = \sum_{t=1}^{T} n_t$ and $n_t \leq n\ \forall t$.
m	Number of temporal basis functions (including the intercept).
L	Number of spatio-temporal model outputs.
p_i	Number of LUR-basis functions for the i:th temporal-basis function (including the intercept).
$l(\Psi, \boldsymbol{\gamma}, \boldsymbol{\alpha}\|Y)$	Log-likelihood for the model (7).
$l_{\text{PROF}}(\Psi\|Y)$	Logarithm of the profile likelihood of $l(\Psi, \boldsymbol{\gamma}, \boldsymbol{\alpha}\|Y)$, (9).

TABLE 4

Cross validation results for the model without and with mean separated, 3km buffer Caline. The table gives RMSE, R^2, and coverage for 95% predictions interval-ls for the cross-validated predictions. For the Home sites the three adjusted R^2:s, showing improvement over simple temporal models, are also provided. All values are computed on the back transformed scale (ppb NO_x).

	No Caline			3km buffer Caline mean separated		
	RMSE	R^2	cov.	RMSE	R^2	cov.
AQS and MESA fixed						
2-week	17.90	0.80	0.91	18.12	0.79	0.90
long-term avg.	11.97	0.58		12.26	0.56	
Snapshot						
2006–07–05	7.94	0.52	0.93	7.62	0.56	0.95
2006–10–25	13.32	0.68	0.97	13.32	0.68	0.95
2007–01–31	15.69	0.66	0.99	15.77	0.66	0.98
Home sites	9.34	0.89	0.97	9.06	0.90	0.95
average		0.67			0.69	
closest		0.74			0.76	
smooth		0.74			0.76	

TABLE 5

Cross validation results, comparing the 3km and 500m buffer Caline. Results are given for original and mean separated Caline. The table gives RMSE and R^2 for the cross-validated predictions. Coverage of the prediction intervals were very similar for both buffer sizes and have been excluded (see Table 4 for coverage using the 3km buffer). All values are computed on the back transformed scale (ppb NO_x).

	3km buffer Caline				500m buffer Caline			
			mean separated				mean separated	
	RMSE	R^2	RMSE	R^2	RMSE	R^2	RMSE	R^2
AQS and MESA fixed								
2-week	18.15	0.79	18.12	0.79	18.34	0.79	17.77	0.80
long-term avg.	12.34	0.55	12.26	0.56	12.26	0.56	12.20	0.56
Snapshot								
2006–07–05	7.57	0.57	7.62	0.56	7.61	0.56	7.43	0.58
2006–10–25	13.51	0.67	13.32	0.68	13.89	0.65	13.47	0.67
2007–01–31	15.99	0.65	15.77	0.66	16.47	0.63	15.84	0.66
Home sites	9.13	0.90	9.06	0.90	9.57	0.89	9.35	0.89

TABLE 6

Cross validation results for the model without and with mean separated, 3km buffer Caline, but excluding all road covariates. The table gives RMSE, R^2, and coverage for 95% predictions intervals for the cross-validated predictions. For the Home sites the three adjusted R^2:s, showing improvement over simple temporal models, are also provided. All values are computed on the back transformed scale (ppb NO_x).

	Without road covariates					
	No Caline			3km buffer Caline mean separated		
	RMSE	R^2	cov.	RMSE	R^2	cov.
AQS and MESA fixed						
2-week	20.42	0.74	0.91	18.40	0.79	0.92
long-term avg.	15.77	0.27		12.74	0.52	
Snapshot						
2006–07–05	9.68	0.29	0.93	8.26	0.48	0.95
2006–10–25	16.51	0.51	0.98	14.90	0.60	0.95
2007–01–31	20.45	0.43	0.98	18.19	0.55	0.96
Home sites	11.00	0.85	0.97	9.31	0.89	0.95
average		0.54			0.67	
closest		0.65			0.75	
smooth		0.64			0.75	

TABLE 7

Estimated parameters, for the models with no Caline compared to mean separated 3km buffer Caline. Both parameter values and standard errors based on the information matrix are given.

	No Caline		3km Caline	
	Est.	Std. err.	Est.	Std. err.
β_1 — Average level				
Intercept	3.78	0.174	3.42	0.207
Distance to road ($\log_{10}$ m)	−0.0801	0.0236	−0.0665	0.0237
Distance to A1 roads ($\log_{10}$ m)	−0.152	0.0323	−0.0630	0.0431
A1 & A2 in 300m buffers (km)	0.0501	0.0253	0.0315	0.0256
A3 in 50m buffers (km)	0.689	0.215	0.781	0.214
Distance to coast (km)	0.0330	0.0102	0.0318	0.00990
Population (1000/2km buffer)	0.00324	0.00117	0.00335	0.00113
Average log(Caline + 1)			0.0789	0.0259
Log Range (log km)	1.86	0.388	1.84	0.384
Log Sill	−2.86	0.287	−2.92	0.283
β_2 — 1st temporal trend				
Intercept	−0.793	0.139	−1.00	0.187
Distance to road ($\log_{10}$ m)	0.00244	0.0259	0.0137	0.0254
Distance to A1 roads ($\log_{10}$ m)	0.0120	0.0274	0.0715	0.0379
A1 & A2 in 300m buffers (km)	0.0437	0.0227	0.0345	0.0214
A3 in 50m buffers (km)	0.136	0.255	0.178	0.245
Distance to coast (km)	0.0221	0.00720	0.0188	0.00753
Population (1000/2km buffer)	−0.00127	0.000782	−0.000949	0.000735
Average log(Caline + 1)			0.0533	0.0227
Log Range (log km)	2.77	0.621	3.34	0.831
Log Sill	−3.82	0.512	−3.55	0.740
β_3 — 2nd temporal trend				
Intercept	−0.142	0.132	−0.204	0.189
Distance to road ($\log_{10}$ m)	0.0503	0.0333	0.0532	0.0329
Distance to A1 roads ($\log_{10}$ m)	−0.0430	0.0326	−0.0263	0.0479
A1 & A2 in 300m buffers (km)	−0.0310	0.0281	−0.0412	0.0264
A3 in 50m buffers (km)	0.338	0.322	0.412	0.309
Distance to coast (km)	0.0130	0.00548	0.0121	0.00581
Population (1000/2km buffer)	−0.0000833	0.000924	0.0000423	0.000896
Average log(Caline + 1)			0.0185	0.0290
Log Range (log km)	2.40	0.646	2.68	0.724
Log Sill	−4.78	0.436	−4.70	0.515
γ				
Mean centered log(Caline + 1)			0.0677	0.0151
ν_{st}				
Log Range (log km)	4.39	0.0938	4.38	0.0935
Log Sill	−3.25	0.0617	−3.25	0.0614
Log Nugget	−4.29	0.0415	−4.30	0.0418

TABLE 8

Estimated parameters, for the models without road covariates but with either no Caline or with the mean separated 3km buffer Caline. Both parameter values and standard errors based on the information matrix are given.

	No Caline		3km Caline	
	Est.	Std. err.	Est.	Std. err.
β_1 — Average level				
Intercept	3.09	0.0826	3.03	0.118
Distance to coast (km)	0.0342	0.00543	0.0304	0.00849
Population (1000/2km buffer)	0.00570	0.000972	0.00394	0.00120
Average log(Caline + 1)			0.145	0.0157
Log Range (log km)	−0.0643	0.528	1.30	0.355
Log Sill	−2.95	0.165	−2.94	0.213
β_2 — 1st temporal trend				
Intercept	−0.755	0.0968	−0.725	0.118
Distance to coast (km)	0.0223	0.00702	0.0188	0.00749
Population (1000/2km buffer)	−0.00121	0.000785	−0.00115	0.000737
Average log(Caline + 1)			0.0256	0.0112
Log Range (log km)	2.70	0.579	3.26	0.805
Log Sill	−3.85	0.472	−3.62	0.708
β_3 — 2nd temporal trend				
Intercept	−0.173	0.0637	−0.172	0.0673
Distance to coast (km)	0.0145	0.00495	0.0134	0.00534
Population (1000/2km buffer)	−0.000275	0.000971	0.0000487	0.000945
Average log(Caline + 1)			0.00350	0.0137
Log Range (log km)	2.04	0.672	2.28	0.655
Log Sill	−4.82	0.367	−4.78	0.413
γ				
Mean centered log(Caline + 1)			0.0738	0.0149
ν_{st}				
Log Range (log km)	4.36	0.0970	4.41	0.0948
Log Sill	−3.24	0.0612	−3.25	0.0611
Log Nugget	−4.32	0.0485	−4.28	0.0420

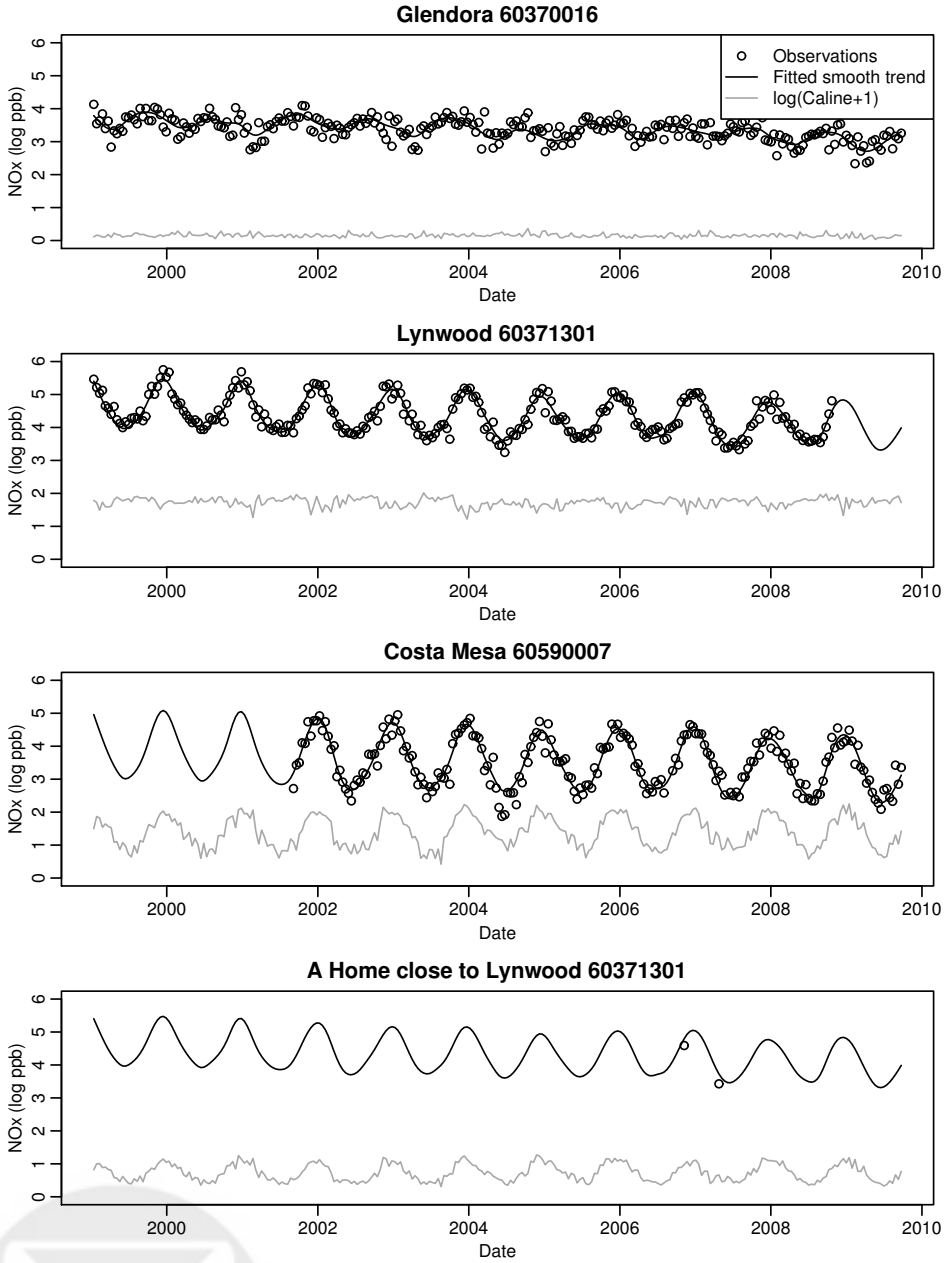

FIGURE 1. *Example time series of log-transformed 2-week average NO_x concentrations at three AQS monitors and one home site in the Los Angeles area. The fit of our smooth temporal basis functions to the data, and the transformed 3km buffer Caline predictions are also shown. For the home site we have used the smooth temporal fit at the closest AQS monitor.*

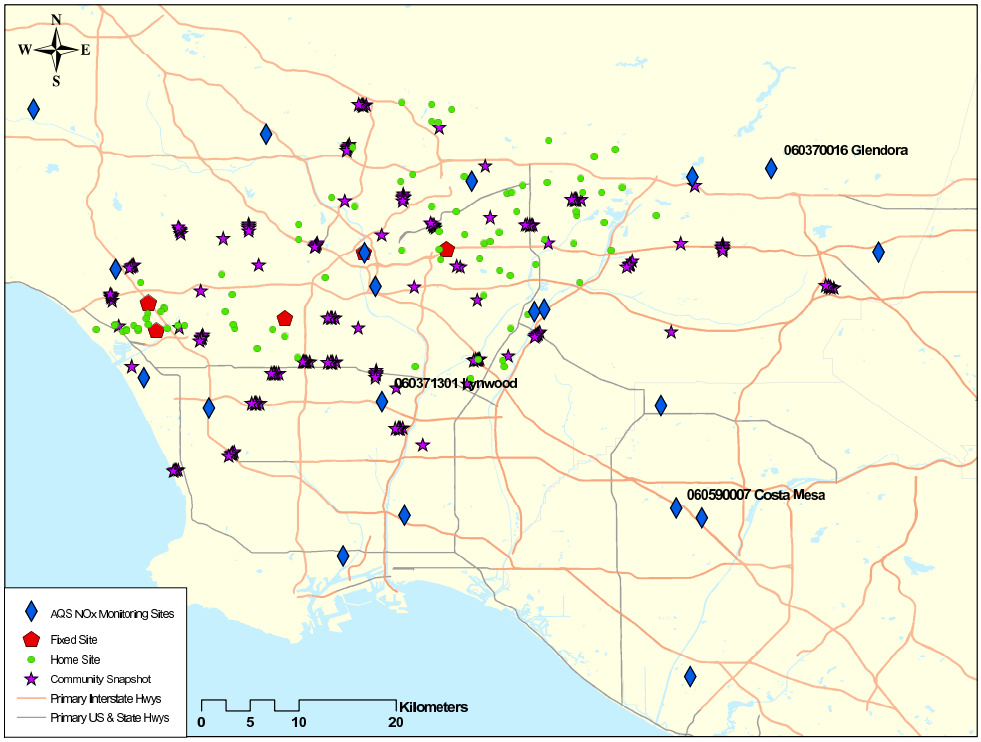

FIGURE 2. *Map illustrating the location of our measurements. The collocated AQS and MESA fixed site are north of the Lynwood AQS site; the MESA fixed site is partially obscured by the AQS sites.*

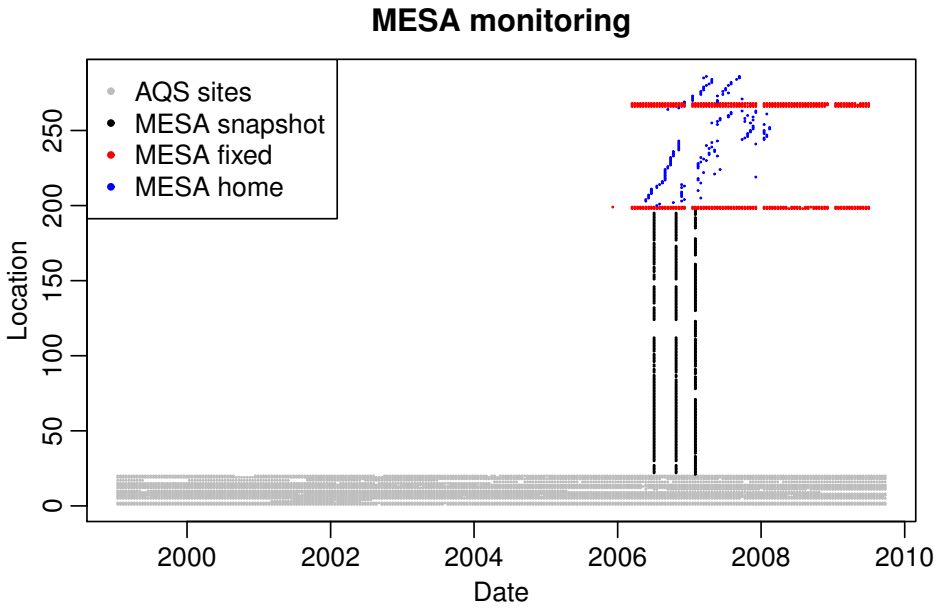

FIGURE 3. *Schematic image of the data available for analysis. Each measurement is represented by a point in space and time. AQS provides temporally rich observations at 20 locations. During the second half of our modeling period, additional temporally rich data are provided by 5 MESA fixed sites. Spatial data are provided by the three MESA snapshot campaigns, which monitored a total of 177 locations at three time points, and by MESA home sites that consists of four monitors alternating among 84 locations.*

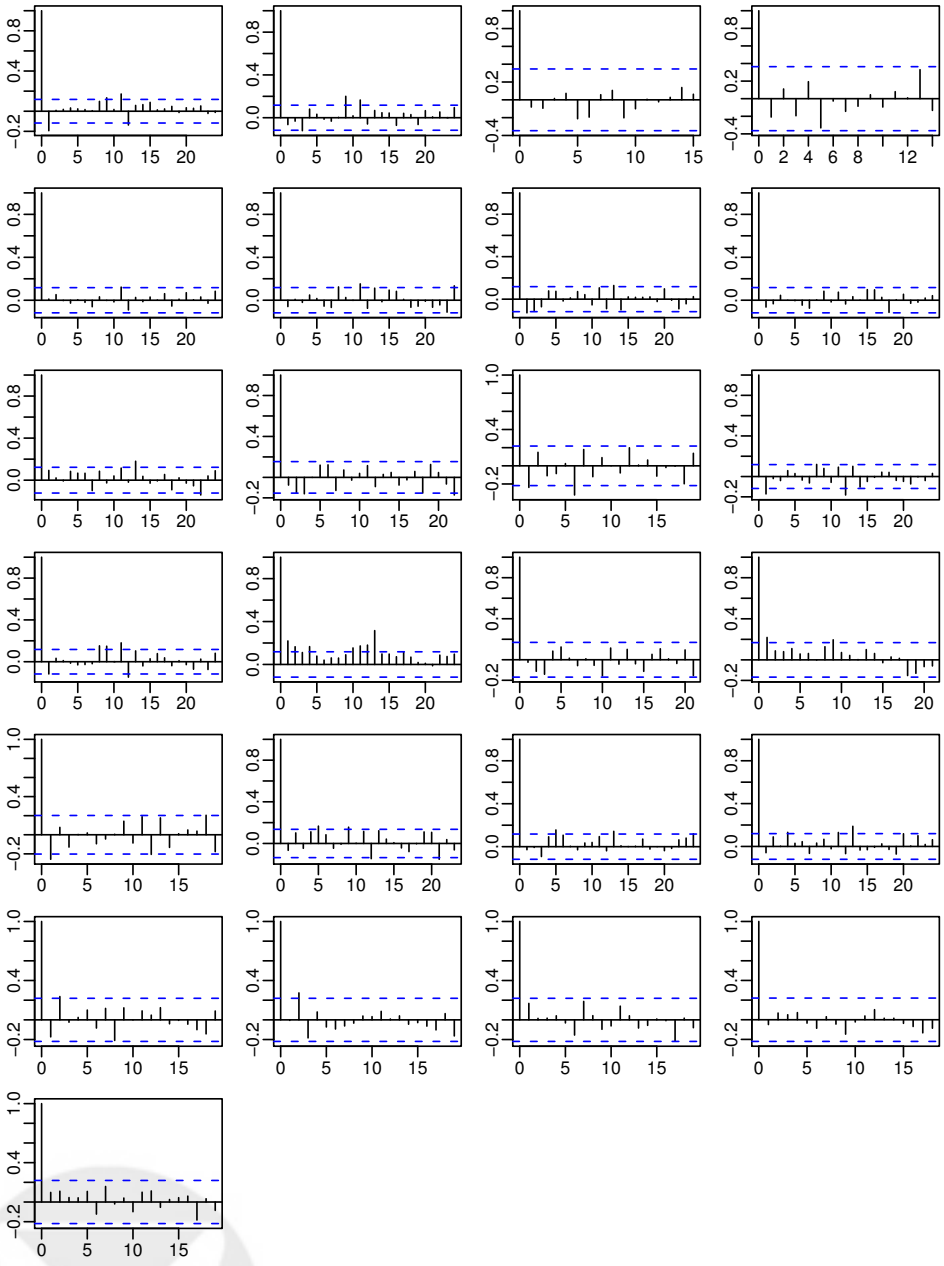

FIGURE 4. *Empirical auto-correlation functions for 2-week average residuals after fitting to the empirical orthogonal basis functions. Results for 20 AQS monitors and 5 MESA fixed sites in Los Angeles area.*

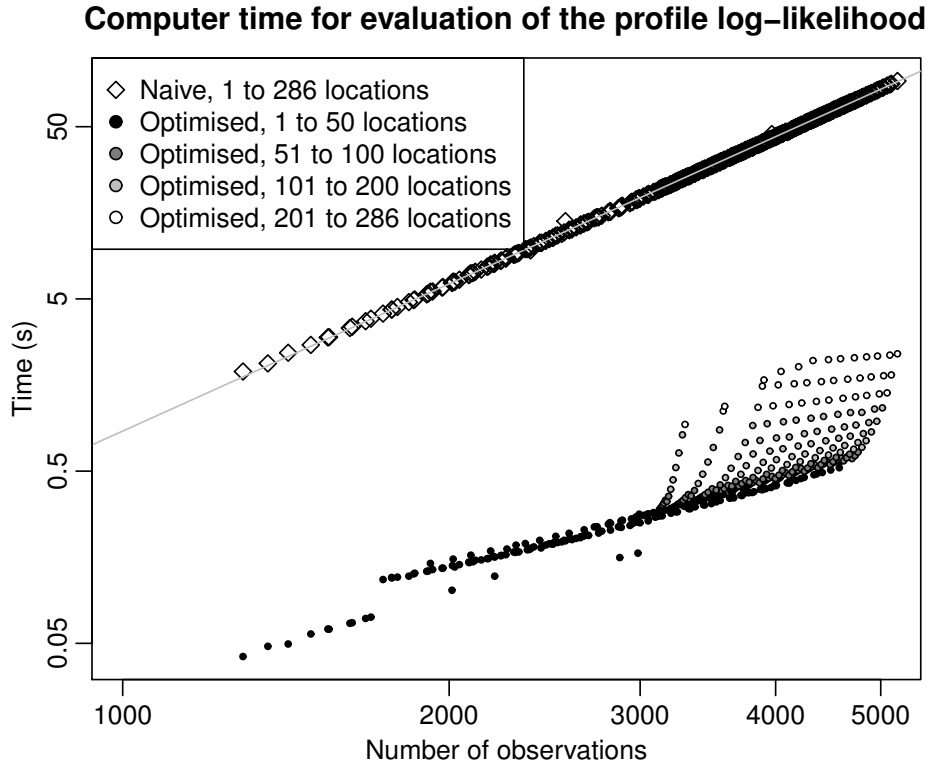

FIGURE 5. *Comparison of the time needed for one evaluation of the naïve profile likelihood* (9) *and simplified version* (12). *The full dataset, 5182 observations from 286 locations and 280 time points, was divided into smaller pieces by dropping either locations and/or time-points to examine how fast the evaluation time would grow as the dataset was expanded. Evaluation time for the full likelihood grows as* $N^{2.8}$ *(the fitted line) close to the expected theoretical value of* $\mathcal{O}\left(N^3\right)$. *For a fixed number of locations evaluation time for the simplified version grows considerably slower than* N^3.

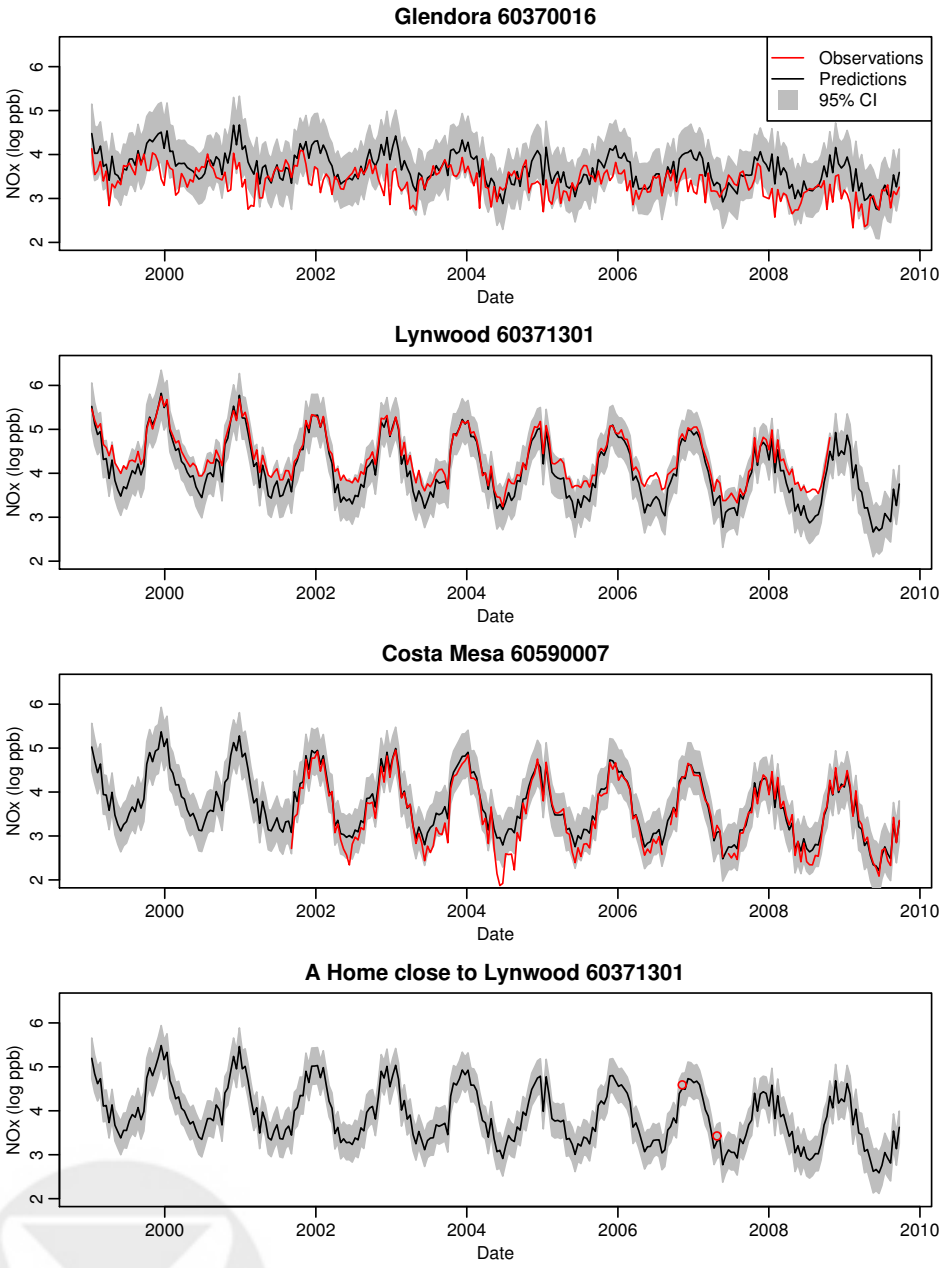

FIGURE 6. *Example of cross-validated predictions of the log-transformed 2-week average NO_x concentrations at three AQS monitors and one home site in the Los Angeles area. Observations, predictions, and 95% prediction intervals are shown.*

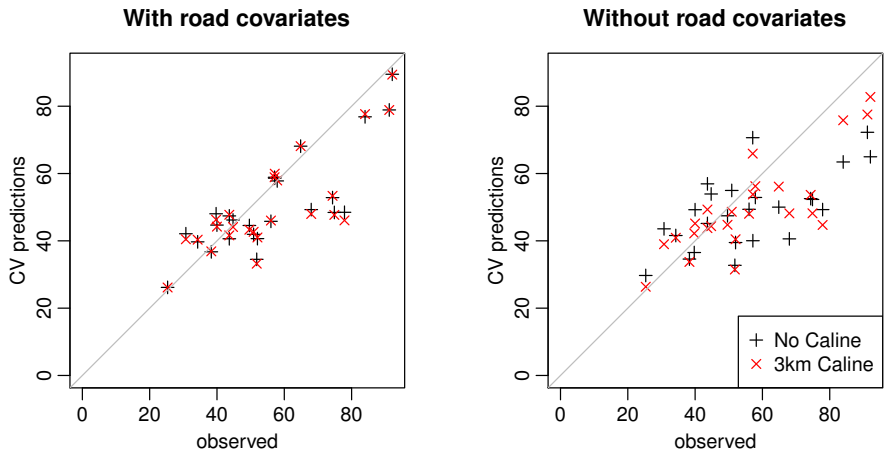

FIGURE 7. *Cross validated predictions for the long-term averages at the AQS and MESA fixed sites. Results for the model both including the road covariates (left) and without the road covariates (right) are given; for both cases predictions without and with the mean separated 3km buffer Caline are shown.*

APPENDIX A: SIMPLIFICATION OF THE LIKELIHOOD

To utilize the block diagonal structure of $\Sigma_\nu(\theta_\nu)$ and $\Sigma_B(\theta_B)$ we rewrite (9) as

$$
\begin{aligned}
2l_{\text{PROF}}(\Psi|Y) = &- \log|\Sigma_\nu(\theta_\nu)| - \log|\Sigma_B(\theta_B)| - \log\left|\Sigma^{-1}_{B|Y}(\Psi)\right| \\
&+ Y^\top\widehat{\Sigma}(\Psi)\mathcal{M}\Big(\mathcal{M}^\top\widehat{\Sigma}(\Psi)\mathcal{M}\Big)^{-1}\mathcal{M}^\top\widehat{\Sigma}(\Psi)Y \\
&- Y^\top\widehat{\Sigma}(\Psi)Y + \text{const.}
\end{aligned} \tag{12}
$$

where const. contains all terms not depending on Ψ, and

$$
\begin{aligned}
\Sigma^{-1}_{B|Y}(\Psi) &= \Sigma^{-1}_B(\theta_B) + F^\top\Sigma^{-1}_\nu(\theta_\nu)F, && \text{(13a)}\\
\Sigma^{-1}_{\alpha|Y}(\Psi) &= X^\top\Sigma^{-1}_B(\theta_B)X - X^\top\Sigma^{-1}_B(\theta_B)\Sigma_{B|Y}(\Psi)\Sigma^{-1}_B(\theta_B)X, && \text{(13b)}\\
\widehat{\Sigma}(\Psi) &= \Sigma^{-1}_\nu(\theta_\nu) - \Sigma^{-1}_\nu(\theta_\nu)F\Sigma_{B|Y}(\Psi)F^\top\Sigma^{-1}_\nu(\theta_\nu) \\
&\quad -\Big[\Sigma^{-1}_\nu(\theta_\nu)F\Sigma_{B|Y}(\Psi)\Sigma^{-1}_B(\theta_B)X\Sigma_{\alpha|Y}(\Psi) && \text{(13c)}\\
&\quad X^\top\Sigma^{-1}_B(\theta_B)\Sigma_{B|Y}(\Psi)F^\top\Sigma^{-1}_\nu(\theta_\nu)\Big].
\end{aligned}
$$

A.1. Proof of equivalence. To prove the equivalence of the two likelihood forms (9) and (12) we will need the following Lemmas:

LEMMA 1. *Blockwise inversion (Thm. 8.5.11 Harville, 1997):*
Let A, B, C, and D be block matrices, with A and $(D - CA^{-1}B)$ being nonsingular, then

$$
\begin{bmatrix} A & B \\ C & D \end{bmatrix}^{-1} = \begin{bmatrix} A^{-1} + A^{-1}B(D-CA^{-1}B)^{-1}CA^{-1} & -A^{-1}B(D-CA^{-1}B)^{-1} \\ -(D-CA^{-1}B)^{-1}CA^{-1} & (D-CA^{-1}B)^{-1} \end{bmatrix}.
$$

LEMMA 2. *Blockwise determinant (Thm. 13.3.8 Harville, 1997):*
Let A, B, C, and D be block matrices, with A and $(D - CA^{-1}B)$ being nonsingular, then

$$
\begin{vmatrix} A & B \\ C & D \end{vmatrix} = |A|\left|D - CA^{-1}B\right|.
$$

LEMMA 3. *The Woodbury identity (Thm. 18.2.8 Harville, 1997):*
If A and B are two invertable matrices of size n-by-n and p-by-p respectively, and C is an arbitrary n-by-p matrix, then

$$
\left(A + CBC^\top\right)^{-1} = A^{-1} - A^{-1}C\left(B^{-1} + C^\top A^{-1}C\right)^{-1}C^\top A^{-1}.
$$

LEMMA 4. *The Searle identity (Thm. 18.2.3 Harville, 1997): If A, B are matrices of size p-by-n and n-by-p respectively, $\mathbf{I}$ denotes identity matrices of appropriate size, and $(\mathbf{I}+AB)$ is nonsingular, then*

$$(\mathbf{I}+AB)^{-1}A = A(\mathbf{I}+BA)^{-1}.$$

LEMMA 5. *If Σ_1 and Σ_2 are two nonsingular matrices of size n_1-by-n_1 and n_2-by-n_2 respectively, and A is a n_2-by-n_1 matrix, then:*

$$\left|A\Sigma_1 A^\top + \Sigma_2\right| = |\Sigma_1|\,|\Sigma_2|\left|\Sigma_1^{-1} + A^\top\Sigma_2^{-1}A\right|.$$

(Thm. 18.1.1 Harville, 1997)

To make the notation clearer we have suppressed the matrices dependence on Ψ in the following. Superscripts above equality signs are used to denote the identities used in each step.

First we note that

$$\text{(14a)}\quad \widetilde{\Sigma}^{-1} = \left(\Sigma_\nu + F\Sigma_B F^\top\right)^{-1} \overset{\text{Lem. 3}}{=} \Sigma_\nu^{-1} - \Sigma_\nu^{-1}F\Sigma_{B|Y}F^\top\Sigma_\nu^{-1},$$

$$\text{(14b)}\quad F^\top\widetilde{\Sigma}^{-1}F \overset{\text{Lem. 3}}{=} \Sigma_B^{-1} - \Sigma_B^{-1}\Sigma_{B|Y}\Sigma_B^{-1},$$

$$\text{(14c)}\quad \widetilde{\Sigma}^{-1}F \overset{\text{Lem. 4}}{=} \Sigma_\nu^{-1}F\Sigma_{B|Y}\Sigma_B^{-1}.$$

Using (14) we have that

$$\text{(15a)}\quad \Sigma_{\alpha|Y}^{-1} \overset{\text{(14b)}}{=} X^\top F^\top\widetilde{\Sigma}_\nu^{-1}FX$$

$$\text{(15b)}\quad \widehat{\Sigma} \overset{\text{(14a) \& (14b)}}{=} -\widetilde{\Sigma}^{-1}FX\Sigma_{\alpha|Y}X^\top F^\top\widetilde{\Sigma}^{-1} + \widetilde{\Sigma}^{-1},$$

For the determinant in (9) we now have that

$$\left|\widetilde{\Sigma}\right| \overset{\text{Lem. 5}}{=} |\Sigma_\nu|\,|\Sigma_B|\left|\Sigma_{B|Y}^{-1}\right|,$$

proving equality of the determinants. For the quadratic form in (9) we have

$$
\begin{aligned}
& Y^\top \widetilde{\Sigma}^{-1}\widetilde{X}\left(\widetilde{X}^\top\widetilde{\Sigma}^{-1}\widetilde{X}\right)^{-1}\widetilde{X}^\top\widetilde{\Sigma}^{-1}Y - Y^\top\widetilde{\Sigma}^{-1}Y \\
\overset{(15a)}{=}\quad & Y^\top \widetilde{\Sigma}^{-1}\widetilde{X}\begin{bmatrix}\Sigma_{\alpha|Y}^{-1} & \mathcal{M}^\top\widetilde{\Sigma}_\nu^{-1}FX \\ X^\top F^\top\widetilde{\Sigma}_\nu^{-1}\mathcal{M} & \mathcal{M}^\top\widetilde{\Sigma}_\nu^{-1}\mathcal{M}\end{bmatrix}^{-1}\widetilde{X}^\top\widetilde{\Sigma}^{-1}Y - Y^\top\widetilde{\Sigma}^{-1}Y \\
\overset{\text{Lem. 1 \& (15b)}}{=}\quad & Y^\top\widetilde{\Sigma}^{-1}\Big[FX\Sigma_{\alpha|Y}X^\top F^\top + \left(\mathbf{I} - FX\Sigma_{\alpha|Y}X^\top F^\top\widetilde{\Sigma}^{-1}\right) \\
& \qquad \mathcal{M}(\mathcal{M}^\top\widehat{\Sigma}\mathcal{M})^{-1}\mathcal{M}^\top\left(\mathbf{I} - \widetilde{\Sigma}^{-1}FX\Sigma_{\alpha|Y}X^\top F^\top\right)\Big]\widetilde{\Sigma}^{-1}Y \\
& -Y^\top\widetilde{\Sigma}^{-1}Y \\
=\quad & Y^\top\Big[\left(\widetilde{\Sigma}^{-1} - \widetilde{\Sigma}^{-1}FX\Sigma_{\alpha|Y}X^\top F^\top\widetilde{\Sigma}^{-1}\right)\mathcal{M}(\mathcal{M}^\top\widehat{\Sigma}\mathcal{M})^{-1}\mathcal{M}^\top \\
& \qquad \left(\widetilde{\Sigma}^{-1} - \widetilde{\Sigma}^{-1}FX\Sigma_{\alpha|Y}X^\top F^\top\widetilde{\Sigma}^{-1}\right) \\
& \qquad - \left(\widetilde{\Sigma}^{-1} - \widetilde{\Sigma}^{-1}FX\Sigma_{\alpha|Y}X^\top F^\top\widetilde{\Sigma}^{-1}\right)\Big]Y \\
\overset{(15b)}{=}\quad & Y^\top\widehat{\Sigma}\mathcal{M}\left(\mathcal{M}^\top\widehat{\Sigma}\mathcal{M}\right)^{-1}\mathcal{M}^\top\widehat{\Sigma}Y - Y^\top\widehat{\Sigma}Y,
\end{aligned}
$$

showing that quadratic forms in (9) and (12) are equal. Given the equality of both determinants and quadratic forms we have now shown that all terms in (9) and (12) that depend on Ψ are equal.

A.2. Computational advantage. At a first glance it is not obvious that (12) is an improvement on (9), but it allows a much more efficient use of the block structure in $\Sigma_B(\theta_B)$ and $\Sigma_\nu(\theta_\nu)$. As an example the matrix $\widetilde{\Sigma}(\Psi)$ in (9) is a dense $N \times N$-matrix, implying that the computational effort of calculating

$$-\log\left|\widetilde{\Sigma}(\Psi)\right|$$

grows at a rate of $\mathcal{O}\left(N^3\right)$. The corresponding term in (12),

$$-\log\left|\Sigma_\nu(\theta_\nu)\right| - \log\left|\Sigma_B(\theta_B)\right| - \log\left|\Sigma_{B|Y}^{-1}(\Psi)\right|,$$

consists of the determinant of two block diagonal matrices and the determinant of a dense $mn \times nm$-matrix. The computational effort scales as

$$\mathcal{O}\left(\sum_{t=1}^{T} n_t^3\right), \quad \mathcal{O}\left(mn^3\right), \quad \text{and} \quad \mathcal{O}\left(m^3n^3\right)$$

for the three components respectively. For our data the term requiring $\mathcal{O}\left(m^3n^3\right)$ computer time will be the most time consuming. Due to the long time period covered and the few temporal basis functions needed we have $mn \ll N$, implying that (12) should be considerably faster to evaluate than (9). It should be noted that with a more balanced sampling design the term requiring $\mathcal{O}\left(\sum_t n_t^3\right)$ is likely to dominate over $\mathcal{O}\left(m^3n^3\right)$. However, we note that $\sum_t n_t^3 \leq N^3$, and (12) should still be faster to evaluate than (9). Similair arguments can be made for the rest of the terms in the log-likelihood, and it can be shown that the overall computational cost of (9) will grow as $\mathcal{O}\left(N^3\right)$, compared to $\mathcal{O}\left(m^3n^3\right)$ (or $\mathcal{O}\left(\sum_t n_t^3\right)$) for (12). A comparison of evaluation times is presented in Figure 5.

APPENDIX B: RESTRICTED MAXIMUM LIKELIHOOD

The REML of (6) can be found in Harville (1974) and taking logarithms we have

$$
\begin{aligned}
2l_{\text{REML}}(\Psi|Y) = &-\left(N - \sum_{i=1}^{m} p_i - L\right)\log(2\pi) - \log\left|\widetilde{\Sigma}(\Psi)\right| + \log\left|\widetilde{X}^\top\widetilde{X}\right| \\
&- \log\left|\widetilde{X}^\top\widetilde{\Sigma}^{-1}(\Psi)\widetilde{X}\right| - Y^\top\widetilde{\Sigma}^{-1}(\Psi)Y \\
&+ Y^\top\widetilde{\Sigma}^{-1}(\Psi)\widetilde{X}\left(\widetilde{X}^\top\widetilde{\Sigma}^{-1}(\Psi)\widetilde{X}\right)^{-1}\widetilde{X}^\top\widetilde{\Sigma}^{-1}(\Psi)Y.
\end{aligned} \tag{16}
$$

The likelihood simplifications outlined in Appendix A can of course also be applied to the REML in (16). First we note that, apart from constants not depending on the Ψ, (9) and (16) only differ by the determinant $\left|\widetilde{X}^\top\widetilde{\Sigma}^{-1}\widetilde{X}\right|$. Further $\widetilde{X}^\top\widetilde{\Sigma}^{-1}\widetilde{X}$ is a block matrix and we have that

$$
\left|\widetilde{X}^\top\widetilde{\Sigma}^{-1}\widetilde{X}\right| \overset{\text{Lem. 2 \& (15)}}{=} \left|\Sigma_{\alpha|Y}^{-1}\right|\left|\mathcal{M}^\top\widehat{\Sigma}\mathcal{M}\right|,
$$

showing that the simplification of (16) is given by adding

$$
-\log\left|\mathcal{M}^\top\widehat{\Sigma}(\Psi)\mathcal{M}\right| - \log\left|\Sigma_{\alpha|Y}^{-1}(\Psi)\right|
$$

to (12).